Wall loss of semi-volatile organic compounds in a Teflon bag chamber for the temperature range of 262-298 K: mechanistic insight on temperature dependence

Longkun He[1], Wenli Liu[2], Yatai Li[1,3], Jixuan Wang[1], Mikinori Kuwata[2], Yingjun Liu[1]

[1]State Key Joint Laboratory of Environmental Simulation and Pollution Control, College of Environmental Sciences and Engineering, Peking University, Beijing, 100871, China

[2]Department of Atmospheric and Oceanic Sciences and Laboratory for Climate and Ocean-Atmosphere Studies, School of Physics, Peking University, Beijing 100871, China

[3]Now at College of Public Health, Zhengzhou University, Zhengzhou, 450001, China

Correspondence to: Mikinori Kuwata (kuwata@pku.edu.cn), Yingjun Liu (yingjun.liu@pku.edu.cn)

Abstract. Teflon bag chambers have long been used for investigating atmospheric chemical processes, including secondary organic aerosol formation. The wall-loss process of gas-phase species in Teflon bag chambers has typically been investigated at around room temperature. Recent laboratory studies started employing Teflon bag chambers at sub-273 K conditions for simulating wintertime and upper tropospheric environments. However, temperature dependence in vapor wall-loss processes of semi-volatile organic compounds (SVOCs) in a Teflon bag chamber has not well been investigated. In this study, we experimentally investigated wall-loss process of C_{14}-C_{19} *n*-alkanes in a 1 m^3 Teflon bag for the temperature range of 262 to 298 K. Enhanced wall losses of the tested *n*-alkanes were observed following the decrease in temperature. For instance, 65% of C_{14} *n*-alkane was lost to the wall 15 hours after injection at room temperature, while the corresponding value was 95% at 262 K. The experimental data were analyzed using the two-layer kinetic model, which considers both absorption of gas phase species to the surface layer of Teflon wall and diffusion to the inner layer. The experimental data demonstrated that absorption of gas phase species by the surface layer enhanced at lower temperature. The temperature dependence in absorption was well accounted using the equilibrium dissolution model of organic compounds to the Teflon surface by considering reduced saturation vapor pressure at lower temperature. On the contrary, diffusion of *n*-alkanes from the surface to inner layer slowed down at reduced temperature. Mechanistic studies on these processes will need to be conducted in the future to quantitatively predict the influence of temperature-dependent wall-loss processes of SVOCs on laboratory experimental results.

1 Introduction

The environmental chamber is one of the most widely-used laboratory systems for studying chemical processes in the atmosphere, including formation of secondary organic aerosol (SOA) (Clark et al., 2016; Nakao et al., 2011; Ng et al., 2007; Song et al., 2005). The environmental chambers are typically made of Teflon films or stainless steel (Cocker et al., 2001; Voigtlaeander et al., 2012). Existence of walls in the environmental chambers induces losses of both vapors and particles due to their deposition on wall surfaces (Mcmurry and Grosjean, 1985; Krechmer et al., 2020). Wall loss of gas-phase organic compounds in the environmental chambers can lead to underestimation of SOA mass yields. For instance, injection of seed particles into Teflon bag has been shown to increase SOA yields by a few times due to the reduced relative importance of the chamber wall as a condensation sink in the system (Kroll et al., 2007; Zhang et al., 2014).

Vapor wall loss in Teflon bag chambers, especially that for semi-volatile organic compounds (SVOCs), has been intensively investigated in the last decade (Matsunaga and Ziemann, 2010; Yeh and Ziemann, 2014, 2015; Zhang et al., 2015; Krechmer et al., 2016; Huang et al., 2018b; Pratap et al., 2020; Yu et al., 2022). For instance, Matsunaga and Ziemann (2010) studied wall-loss process of alkanes, alkenes, alcohols, and ketones. These previous wall-loss experiments were dominantly conducted at around room temperature (293~303 K), as most of the chamber studies employed the corresponding temperature range (Hidy, 2019). The experimental results were often modeled by assuming equilibrium dissolution of the organic compounds into the Teflon film. A more recent study separately considered the surface and inner layer of the Teflon film for explaining the loss process more quantitatively (Huang et al., 2018b).

Recently, a growing number of environmental chamber experiments have been conducted at low temperatures to simulate wintertime/upper tropospheric conditions in laboratory (Huang et al., 2018a; Pratap et al., 2019; Quelever et al., 2019; Simon et al., 2020; Wang et al., 2022). For instance, some SOA formation experiments have been conducted for the temperature range down to 223 K using stainless steel chambers such as the Aerosol Interaction and Dynamics in the Atmosphere (AIDA) and Cosmics Leaving OUtdoor Droplets (CLOUD) chambers (Huang et al., 2018a; Simon et al., 2020). Teflon bag chambers have also been employed for the temperature range down to 258 K (Kristensen et al., 2017; Deng et al., 2021). These studies demonstrate that temperature is an important parameter determining both mass yields and chemical composition of SOA. Vapor wall loss of SVOCs in the environmental chambers for the corresponding temperature range needs to be understood for better interpreting these experimental data in a quantitative way. So far only one group attempted to investigate vapor wall loss below room temperature, by measuring the size evolution of levoglucasan particles injected into a Teflon chamber (Pratap et al., 2020). However, the experimental results were confounded by slow evaporation of levoglucosan from particles at low temperatures.

This study investigated vapor wall loss of C_{14}-C_{19} n-alkanes in a Teflon chamber for the temperature range of 262 to 298 K by monitoring the evolution of their gas-phase concentrations following a pulse release. The wall-loss process was

58 investigated as a function of temperature. The experimental results were analyzed using the two-layer kinetic model, which

59 considers partitioning of gas phase SVOCs to the surface layer, as well as further diffusion to the inner layer. Temperature

60 effects on the two processes were evaluated separately.

61 **2 Experimental**

62 **2.1 Teflon chamber experiments**

63   Figure 1 shows the experimental setup. The experiment was conducted using a fluorinated ethylene propylene (FEP)

64 bag with the volume of 1 m^3. The thickness of the FEP film for the bag was 75 μm. The dimension of the bag was 260 cm ×

65 55 cm × 70 cm. The area to volume ratio of the chamber was 7.26 m^{-1}. The chamber volume was experimentally validated by

66 employing CO_2 as a tracer (Figure S1). The timescale for CO_2 to be well mixed in the bag after a pulse injection was

67 approximately 30 mins (Figure S1). The bag was newly purchased for the experiment, meaning that it was employed for no

68 other experiments. The bag was installed in a chest freezer (Type 2288, Nixue Inc.), which was equipped with an additional

69 internal thermal insulation layer. Two fans were installed in the freezer (outside the bag) to facilitate mixing of air so that air

70 temperature in the freezer was uniform. The temperature of the freezer was measured at 3 points using temperature sensors

71 (Figure 1). Temporal variation of temperature was ± 0.5 K at 262 K.

72   Throughout the experiments, purified air was employed. The purified air was produced using a zero air generator

73 (Model 747−30, AADCO Instruments, Inc.) and further purified using a hydrocarbon trap (BHT-2, Agilent Technologies, Inc.).

74 Hydrocarbon concentration in the purified air was less than 5 ppbv. Relative humidity (RH) was less than 0.1%.

75   Solutions containing C_{14} - C_{19} *n*-alkanes (Konoscience Inc., > 98%) were prepared and injected into the chamber.

76 Hexane (Fisher Chemical Co., HPLC grade) was employed as the solvent. The purities and saturation vapor pressures of all

77 chemicals are given in Table S1. The solutions were injected to the chamber using a syringe pump (Fusion 200 Touch, Chemyx

78 Inc.) and a nebulizer (TR-30-A1, Meinhard Inc.) through polytetrafluoroethylene (PTFE) tubing, as shown in Figure 1. The

79 use of nebulizer expedited the evaporation of the solution.

80   Eight sets of wall-loss experiments were conducted in the temperature range of 262 to 298 K. Prior to each experiment,

81 the chamber was heated to ~320 K and continuously flushed using purified air. The cleaning process lasted for 2~3 days until

82 the concentration of investigated *n*-alkanes dropped to the background level. To start an experiment, the chamber was switched

83 to batch mode and the solution was injected to the chamber at room temperature. The injection lasted for 13 mins, with a liquid

84 flow rate of 100 μL min^{-1}. The air flow rate of the nebulizer was 0.7 L min^{-1}. The resulting initial concentrations (C_0) of

85 individual *n*-alkanes in the chamber ranged from 4 to 50 μg m^{-3} assuming no wall loss, which were lower than 20% of their

86 saturation concentrations under the corresponding experimental temperature to avoid particle formation. The solution used for

87 low-temperature experiments (< 278 K) did not contain C_{18} and C_{19} *n*-alkanes to avoid formation of particles. For experiments

88   below room temperature, the cooling system of the freezer was turned on one hour after the completion of the injection. The

89   operation procedure was employed to avoid homogeneous nucleation and subsequent condensational growth of aerosol

90   particles. The validity of employing this post-cooled operation procedure was demonstrated by comparison with a pre-cooled

91   chamber result at 270 K (Figure S2). Measurements using an optical particle counter (11-D, GRIMM Aerosol Technik Ainring,

92   Germany) experimentally confirmed negligible abundance of aerosol particles in the chamber ($< 0.5 \, \mu g \, m^{-3}$). It took ~3 hours

93   for the temperature in the freezer to drop to a stable level after injection (Figure S3). Although the air in the bag leaked out

94   during experiments due to compression of the bag by its own weight, absence of intrusion of room air to the bag was confirmed

95   by observing no changes in contaminant signals (Table S2). The gas-phase concentrations of n-alkanes were therefore

96   unaffected by the changes in bag volume.

97   Concentrations of SVOCs in the chamber were quantified using the semi-volatile thermal desorption aerosol gas

98   chromatograph (SV-TAG, Aerodyne Research Inc. & Aerosol Dynamic Inc., USA) (Zhao et al., 2013). The gas

99   chromatography-mass spectrometer (GC-MS) (7890B, Agilent Technologies, Inc.) was employed for the system. Detailed

100 descriptions of the SV-TAG operation and performance tests were presented in our previous papers (Li et al., 2022a; Li et al.,

101 2022b). Herein, chamber air was sampled through ~1 m long perfluoroalkoxy alkane (PFA) tubing (1/4 inch in diameter). Prior

102 to sampling, the chamber air passed through the PFA tubing at 0.5 L min^{-1} for at least 20 min for passivating the tubing wall

103 (Matsunaga and Ziemann, 2010). Samples were periodically collected for 5 min at 4 L min^{-1} for each time at 1-15 hours after

104 injection. As the absence of particles was confirmed, only gas-phase SVOCs were sampled by the SV-TAG. The instrument

105 response to n-alkanes was calibrated with standards before and after each experiment (Figure S4), utilizing the in-situ automatic

106 injection system (Isaacman et al., 2011). The gas-phase concentrations of SVOCs were calculated from the measured quantity

107 of SVOCs and sampled air volume.

2.2 Kinetic model

109   Herein we used a unified vapor wall-loss transport model developed by Huang et al. (2018b) to fit the experimental

110 data. Figure 2 shows the concept of the model. Briefly, SVOCs partition between the gas phase and the surface of the FEP

111 film. Subsequently, the absorbed SVOCs may diffuse to the inner layer of the film. As the thickness of the FEP film (75 μm)

112 is a couple of orders larger than that of the surface layer (~ 5 nm) (Huang et al., 2018b), the inner layer is assumed as an

113 infinite sink. As a result, the diffusion process of SVOCs from the inner layer to the film surface is ignored. A list of all the

114 parameters is provided in Nomenclature. The governing equations without and with considering diffusion to the inner layer

115 are presented below, respectively.

116   (1) Without considering the diffusion process in the inner layer, the wall loss process is solely controlled by

117 partitioning of SVOCs between the gas phase and surface layer and can be described as follows

118
$$\text{Gas phase} \underset{k_{-1}}{\overset{k_1}{\rightleftharpoons}} \text{Surface} \tag{1}$$
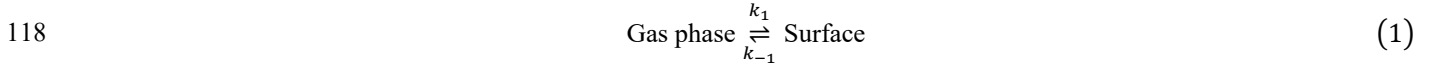
119 where k_1 and k_{-1} are forward and backward rate constants in the process. The corresponding first-order kinetic equations are

120
$$\frac{dC_{gas}}{dt} = -k_1 C_{gas} + k_{-1} C_{surface}$$
$$\frac{dC_{surface}}{dt} = k_1 C_{gas} - k_{-1} C_{surface} \tag{2}$$

121 where C_{gas} and $C_{surface}$ are the SVOC concentrations in gas phase and on wall surface, respectively. It should be noted that
122 $C_{surface}$ was defined as the total mass of SVOC on wall surface divided by the chamber volume, following previous studies
123 (Matsunaga and Ziemann, 2010; Yeh and Ziemann, 2014, 2015). This model has been commonly used to interpret the
124 experimental data of vapor wall loss in previous studies (Matsunaga and Ziemann, 2010; Yeh and Ziemann, 2014, 2015;
125 Zhang et al., 2015).

126 The gas-surface equilibrium time scale $\tau_{surface}$ and equilibrium constant K_{eq} can be obtained by

127
$$\tau_{surface} = \frac{1}{k_1 + k_{-1}} \tag{3}$$

128
$$K_{eq} = \frac{k_1}{k_{-1}} = \left[\frac{C_{surface}}{C_{gas}}\right]_{eq} \tag{4}$$

129 (2) Considering the diffusion process in the inner layer, the whole vapor wall loss process can be formulated as
130 follows

131
$$\text{Gas phase} \underset{k_{-1}}{\overset{k_1}{\rightleftharpoons}} \text{Surface} \overset{k_2}{\rightarrow} \text{Inner Layer} \tag{5}$$
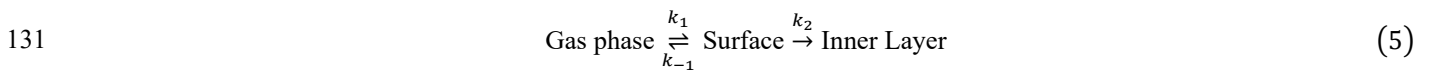
132 where k_2 is the first-order loss rate constant in the diffusion process. Correspondingly, the kinetic processes for C_{gas} and
133 $C_{surface}$ can be described by the following equations

134
$$\frac{dC_{gas}}{dt} = -k_1 C_{gas} + k_{-1} C_{surface}$$
$$\frac{dC_{surface}}{dt} = k_1 C_{gas} - k_{-1} C_{surface} - k_2 C_{surface} \tag{6}$$

135   The diffusion process has the first-order decay time scale τ_{inner} of $\tau_{inner} = \frac{1}{k_2}$. If $k_2 \ll k_1 + k_{-1}$ (i.e., $\tau_{inner} \gg \tau_{surface}$),

136   gas-surface partitioning occurs much faster than the diffusion process to the inner layer. In this case, the apparent first-order

137   decay loss constant of SVOC from the gas phase can asymptotically be represented as (Huang et al., 2018b):

$$\frac{dC_{gas}}{C_{gas}dt} \approx -\frac{K_{eq}}{1 + K_{eq}}k_2 \qquad (7)$$

139   The data analysis and model fitting were conducted using Wolfram Mathematica 13.1. The controlling factors of

140   individual parameters in the above equations were previously discussed by Huang et al. (2018b).

3 Results and discussion

3.1 Wall loss of *n*-alkanes at room temperature

143   An example of temporal profile for C_{14}-C_{19} *n*-alkanes during the experiment at 298 K is shown in Figure 3. The figure

144   demonstrates the temporal change of C_{gas}/C_0, where C_0 indicates the initial concentration of *n*-alkanes. The values of C_{gas}/C_0

145   for each *n*-alkane exhibited similar temporal patterns. During the first one hour following the injection, C_{gas}/C_0 exponentially

146   decreased. After that, gradual decreases in C_{gas}/C_0 were observed. For example, the decline in gas fraction for C_{14} *n*-alkane

147   during the first hour accounted for 71% of the total change in C_{gas}/C_0 over the whole experimental period of 15 hours. The

148   values of C_{gas}/C_0 decreased with the increase in carbon number, indicating enhanced wall loss. The values of C_{gas}/C_0 at 15

149   hours after injection were 0.32, 0.25, 0.16, 0.097, 0.069, and 0.037 for C_{14} - C_{19} *n*-alkanes, respectively.

150   The experimental result can be well fitted using the two-layer model, but the fits deteriorate in the case that diffusion

151   in the inner layer is neglected (Figure 3). The optimized parameter sets are shown in Table S3. Mass fractions of injected

152   chemical species in the gas, surface, and inner layer phases that were estimated using the model are shown in Figure S5. In the

153   case of the most volatile compound (C_{14} *n*-alkane), the maximum mass fraction in the surface phase occurred at 2 hours after

154   injection. Subsequently, the mass fractions for the compound in both gas phase and surface layer gradually decreased. During

155   this period, the ratio of the mass in the surface layer to that in the gas phase stabilized at 1.33. The mass fraction of the

156   compound in the inner layer steadily increased, reaching 0.22 at 15 hours after injection.

157   In the case of the least volatile compound (C_{19} *n*-alkane), the mass fraction in the surface layer reached the maximum

158   (~76%) approximately 1 hour after injection, accounting for the rapid decrease in the observed concentration in the gas phase.

159   Subsequently, mass fractions of the compound in the gas phase and in the surface layer decreased in proportion. The

160   concentration ratio of the gas phase and surface layer stayed constant (Figure S5). The mass fraction of the compound in the

161   inner layer kept increasing during the experiment. At 15 hours after injection, 87% of the compound existed in the inner layer.

162   The time scale for n-alkanes to reach partitioning equilibrium between the gas and surface phases is estimated to be
163   12 ~ 35 mins, consistent with literature data. For example, Matsunaga and Ziemann (2010) reported that the corresponding
164   time scale for C_8 - C_{16} alkanes was 60 ± 20 mins. The corresponding value for oxygenated organic compounds was reported
165   as 26 ± 23 mins (Yeh and Ziemann, 2015).

166   Our result for the mass transfer of SVOCs to the inner layer can also be compared with a previous study. The rates
167   for the decrease in C_{gas}/C_0 for C_{14}-C_{19} n-alkanes were 0.6–1.3% hour^{-1} after the partitioning between gas phase and surface
168   layer reached equilibrium (*i.e.*, 3 ~ 15 hours). Yeh and Ziemann (2015) reported the corresponding value for 2-ketones as
169   approximately 1% hour^{-1} for the time scale of 7 hours. They suggested that the value is close to the theoretical value for the
170   Fickian diffusion loss rate (~0.5 % hour^{-1}).

3.2 Temperature dependence of wall loss of n-alkanes

172   Figure 4a summarizes the values of C_{gas}/C_0 for all experiments at 3 hours after injection. The data for this sampling
173   time were selected, as the loss of gas phase species by partitioning to the surface layer accounted for the dominant portion of
174   the decline in the gas phase concentration. Generally, C_{gas}/C_0 was lower for less volatile compounds and at lower temperature,
175   suggesting enhanced partitioning of n-alkanes to the chamber wall. The data for the room temperature (C_{gas}/C_0 = 0.47, 0.45,
176   0.34, 0.24, 0.17, and 0.091 for C_{14}, C_{15}, C_{16}, C_{17}, C_{18}, and C_{19} n-alkanes) were smaller than that have been reported by a
177   previous study. Namely, Matsunaga and Ziemann (2010) quantified the corresponding values for equilibration between the
178   gas and surface phases for C_{14}-C_{16} n-alkanes as ~80 – 90%. The enhanced partitioning to the surface layer in our study is likely
179   due to that the chamber for the present study has a larger area to volume ratio (7.26 m^{-1} versus 3.39 m^{-1}).

180   Figure 4b shows the values of C_{gas}/C_0 as a function of temperature at 15 hours after injection. In all experiments, the
181   values of C_{gas}/C_0 at 15 hours after injection were consistently lower than those for 3 hours. For instance, C_{gas}/C_0 for C_{14} n-
182   alkane at 262 K decreased from 0.15 (3 hours) to 0.06 (15 hours). As discussed in the case of the experiment at 298 K, the
183   result suggests that diffusional loss in the inner layer of the chamber wall occurred for the whole temperature range.

3.3 Temperature dependence of partitioning between gas phase and wall surface

185   The temperature dependence in the data summarized in Figure 4a can be understood by considering changes in
186   partitioning between the gas phase and surface layer. Matsunaga and Ziemann (2010) introduced the following equation for
187   relating $C_{surface}/C_{gas}$ and temperature based on the equilibrium dissolution model:

188
$$\left[\frac{C_{surface}}{C_{gas}}\right]_{eq} = K_{eq} = \frac{C_{FEP\_surface}RT}{M_{wall}\gamma_{FEP\_surface}P_s(T)} \qquad (8)$$

189 where $C_{FEP\_surface}$ is the equivalent organic mass concentration of the FEP chamber surface wall, M_{wall} is the average

190 molecular mass of the FEP, $\gamma_{FEP\_surface}$ is the activity coefficient of the organic compound in the Teflon surface, R is the gas

191 constant, and T is temperature. $P_s(T)$ is the saturation vapor pressure of the compound at temperature T. Among the terms for

192 the right-hand-side of equation (8), $RT/P_s(T)$ can be calculated from the experimental conditions. Herein $P_s(T)$ was calculated

193 by the EVAPORATION group contribution method (Compernolle et al., 2011). Comparison between the EVAPORATION

194 method and other approaches for estimating $P_s(T)$ is available in Figure S6. The equation suggests that $[C_{surface}/C_{gas}]_{eq}$ and

195 $RT/P_s(T)$ may vary in proportion, with the slope of $C_{FEP\_surface}/(M_{wall}\gamma_{FEP\_surface})$.

196   It is challenging to retrieve the value of $[C_{surface}/C_{gas}]_{eq}$ by fitting the data of the low-temperature experiments

197 using the two-layer model, since the chamber was cooled after the injection of n-alkanes. Alternatively, the value of

198 $[C_{surface}/C_{gas}]_{eq}$ was approximated using $1/[C_{gas}/C_0]_{\text{at 3 hours}} - 1$, assuming that diffusion of n-alkanes to the inner layer

199 was still a minor loss process within 3 hours. Potential uncertainties associated with this approximation are summarized in

200 Text S1. The uncertainties were estimated in two ways: (1) kinetic simulation based on fitting parameters in Figure 3 (Figure

201 S5) and (2) comparison of the retrieved values of $[C_{surface}/C_{gas}]_{eq}$ ($i.e.$, K_{eq}) and $1/[C_{gas}/C_0]_{\text{at 3 hours}} - 1$ at room

202 temperature (Table S3). The room-temperature experiments were conducted for three runs, allowing for the estimation of

203 experimental uncertainties as standard deviation. Although the kinetic simulation implies overestimates of 7 - 55%, the

204 measurement-based comparison demonstrates that $1/[C_{gas}/C_0]_{\text{at 3 hours}} - 1$ and $[C_{surface}/C_{gas}]_{eq}$ agree within the

205 experimental uncertainties, thereby supporting the validity of the approximation.

206   Figure 5 shows the correlations between $C_{surface}/C_{gas}$ and $RT/P_s(T)$ for individual compounds. For all the tested

207 compounds, these two parameters correlated well, even though $C_{surface}/C_{gas}$ increased by more than one order of magnitude

208 when the chamber was cooled down. The result suggests that equation (8) can be applied to a wide range of temperatures

209 without considering the temperature dependence of $C_{FEP\_surface}/(M_{wall}\gamma_{FEP\_surface})$. In other word, $\gamma_{FEP\_surface}$ can be

210 practically treated as a constant for the investigated temperature range, given $C_{FEP\_surface}$ and M_{wall} are independent of

211 temperature. This implication is consistent with previous findings that the activity coefficients of organic compounds in

212 polymers only change slightly with temperature. For instance, Kontogeorgis et al. (1993) compared the experimental and

213 modelled values of activity coefficients for hydrocarbons in a few polymers such as low-density polyethylene. The values of

214 activity coefficients change by 10~20% for a temperature change of 100 K.

215   Values of $\gamma_{FEP\_surface}$ for n-alkanes can be estimated from Figure 5. Based on equation (8), the fitted slopes

216 correspond to $C_{FEP\_surface}/(M_{wall}\gamma_{FEP\_surface})$. For a specific chamber design, compound-independent $C_{FEP\_surface}$ can be

217 estimated by the density of FEP film (2150 kg m^{-3}) ,the thickness of surface layer ($\sim$ 5 nm), and the surface-to-volume ratio of

218 the chamber (Huang et al., 2018b).The estimated $C_{FEP\_surface}$ for the chamber in this experiment was 78.2 mg m^{-3}. For
219 estimating compound-dependent $\gamma_{FEP\_surface}$, previous studies assumed M_{wall} = 200 g mol^{-1} (Huang et al., 2018b; Matsunaga
220 and Ziemann, 2010). The same approximations were employed in the present study.

221   Figure 6 plots the retrieved values of $\gamma_{FEP\_surface}$ for n-alkanes against $P_s(298\,\text{K})$ for n-alkanes. The figure also
222 shows the corresponding parameters obtained from previous experimental studies (compiled by Huang et al. (2018b), including
223 Matsunaga and Ziemann (2010), Yeh and Ziemann (2014, 2015), and Krechmer et al. (2016)). It should be noted that the
224 literature results were analyzed with fixed values of area to volume ratio of 3 m^{-1} and $C_{FEP\_surface}$ of 32.2 mg m^{-3} (Huang et
225 al., 2018b). Regardless of differences in types of chemicals and chambers, the experimentally estimated values of $\gamma_{FEP\_surface}$
226 and $P_s(298\,\text{K})$ correlate in logarithmic scale. The relationship followed the equation of $\ln(\gamma_{FEP_{surface}}) = 0.40 -$
227  $0.61\ln(P_s(298\,\text{K}))$.

228 **3.4 Characterization of diffusion from the Teflon surface to inner layer**

229   Values of k_2 were estimated using equation (7), since values of τ_{inner} are at least 18 times larger than those of
230 $\tau_{surface}$ (Table S3). The values of C_{gas}/C_0 at 3 hours after injection were employed to calculate K_{eq} as discussed earlier.
231 The experimental data for 9, 12, and 15 hours after injection was employed for obtaining k_2.

232   Figure 7 plots the estimated values of k_2 against $P_s(T)$ for all compounds in all experiments. The values of k_2 and
233 $P_s(T)$ positively correlate. As a comparison point, a previous study reported positive correlations for (1) the diffusivity of
234 organic compounds in FEP film and saturation concentration, and (2) k_2 and diffusivity (Huang et al., 2018b). Our current
235 result is qualitatively similar to the previous study, though temperature was maintained as a constant in the previous study.
236 The decrease in k_2 at lower temperature could be induced by reduced viscosity in the inner layer or weakened thermal motion
237 of n-alkane molecules (Mattila et al., 2023). It should be noted that compression of bag volume during experiment would lead
238 to an increase in the area to volume ratio. Consequently, this could disrupt the relatively slow diffusion process. Based on
239 some photos during the experiment, the leak-out air could have increased the area to volume ratio by a few times. Further
240 study, that considers changes of chamber volume, would be needed in the future for quantitatively interpreting the data.

241 **4 Conclusions**

242   The present study investigated the wall loss process of C$_{14}$-C$_{19}$ n-alkanes to the wall of a 1 m^3 chamber bag, which was
243 composed of FEP film. The temperature of the chamber was controlled for the range of 262 to 298 K. Decay in gas-phase
244 concentrations of the n-alkanes was quantified using the SV-TAG for 15 hours following injection. The temporal variations in
245 the n-alkane concentrations suggested two types of loss processes. The first process was characterized by rapid exponential

246 decay in the first few hours. Subsequently, slow first-order decrease in the n-alkane concentrations was identified until the end
247 of the experiment. Enhanced wall loss was observed at lower temperatures for all compounds.

248   The experimental data were well fitted using the two-layer kinetic model, which considers partitioning of gas-phase
249 species to the surface layer of the chamber film and further diffusion to the inner layer. The analysis suggests that when the
250 Teflon bag chamber is operated at low temperatures, partitioning of gas phase species to the chamber wall surface is enhanced,
251 whereas the permeation of the chemical compounds to the inner layer is suppressed. The temperature effect on gas-surface
252 partitioning overweighs that on diffusion into the inner layer for n-alkanes, leading to an overall enhanced wall loss at lower
253 temperature.

254   The quasi-equilibrium partitioning of n-alkanes between the gas phase and surface layer was interpreted by considering
255 the dissolution process of the species into the surface layer. Values of $C_{surface}/C_{gas}$ at quasi-equilibrium are proportional to
256 $RT/P_s(T)$ for individual compounds. The result suggests that decreased saturation vapor pressure is the major driving force
257 for enhanced partitioning to the surface layer at low temperatures for all investigated compounds, while their activity
258 coefficients can be practically treated as constants for the investigated temperature range. The relationship can be potentially
259 employed for predicting changes in wall loss of SVOCs as a function of temperature, after further verification employing other
260 types of organic compounds.

261   In the future, the underlying mechanisms of the present findings will need to be sought for a better understanding of the
262 chamber wall loss of SVOCs. The present study focused on n-alkanes. In the case of chamber experiments for SOA formation,
263 wall loss processes of oxygenated chemical species would be more important. Thus, a temperature-dependent wall loss study
264 for oxygenated chemical species will still need to be conducted for interpreting SOA chamber experiments under a wide range
265 of temperatures.

266 **Data Availability**

267 Data will be made available on request.

268 **Author contribution**

269 **Longkun He:** Conceptualization, Methodology, Experiment, Data curation, Formal analysis, Writing – original draft. **Wenli**
270 **Liu:** Methodology, Experiment, Writing – review & editing. **Yatai Li:** Methodology, Writing – review & editing. **Jixuan**
271 **Wang:** Experiment, Writing – review & editing. **Mikinori Kuwata:** Conceptualization, Methodology, Project administration,
272 Funding acquisition, Formal analysis, Writing – review & editing, Supervision. **Yingjun Liu:** Conceptualization,
273 Methodology, Project administration, Funding acquisition, Formal analysis, Writing – review & editing, Supervision.

274 **Competing interests**

275 The authors declare that they have no conflict of interest.

276 **Acknowledgements**

277 We thank Dr. Ying Zhou for assisting to improve figure quality. This research was supported by the National Natural

278 Science Foundation of China (92044303, 42175121, and 42150610485).

Reference

Clark, C. H., Kacarab, M., Nakao, S., Asa-Awuku, A., Sato, K., and Cocker, D. R., III: Temperature effects on secondary organic aerosol (SOA) from the dark ozonolysis and photo-oxidation of isoprene, Environ. Sci. Technol., 50, 5564-5571, https://doi.org/10.1021/acs.est.5b05524, 2016.

Cocker, D. R., Flagan, R. C., and Seinfeld, J. H.: State-of-the-art chamber facility for studying atmospheric aerosol chemistry, Environ. Sci. Technol., 35, 2594-2601, https://doi.org/10.1021/es0019169, 2001.

Compernolle, S., Ceulemans, K., and Muller, J. F.: EVAPORATION: A new vapour pressure estimation method for organic molecules including non-additivity and intramolecular interactions, Atmos. Chem. Phys., 11, 9431-9450, https://doi.org/10.5194/acp-11-9431-2011, 2011.

Deng, Y. G., Inomata, S., Sato, K., Ramasamy, S., Morino, Y., Enami, S., and Tanimoto, H.: Temperature and acidity dependence of secondary organic aerosol formation from alpha-pinene ozonolysis with a compact chamber system, Atmos. Chem. Phys., 21, 5983-6003, https://doi.org/10.5194/acp-21-5983-2021, 2021.

Hidy, G. M.: Atmospheric chemistry in a box or a bag, Atmosphere, 10, 401, https://doi.org/10.3390/atmos10070401, 2019.

Huang, W., Saathoff, H., Pajunoja, A., Shen, X. L., Naumann, K. H., Wagner, R., Virtanen, A., Leisner, T., and Mohr, C.: Alpha-pinene secondary organic aerosol at low temperature: Chemical composition and implications for particle viscosity, Atmos. Chem. Phys., 18, 2883-2898, https://doi.org/10.5194/acp-18-2883-2018, 2018a.

Huang, Y. L., Zhao, R., Charan, S. M., Kenseth, C. M., Zhang, X., and Seinfeld, J. H.: Unified theory of vapor-wall mass transport in Teflon-walled environmental chambers, Environ. Sci. Technol., 52, 2134-2142, https://doi.org/10.1021/acs.est.7b05575, 2018b.

Isaacman, G., Kreisberg, N. M., Worton, D. R., Hering, S. V., and Goldstein, A. H.: A versatile and reproducible automatic injection system for liquid standard introduction: Application to in-situ calibration, Atmos. Meas. Tech., 4, 1937-1942, https://doi.org/10.5194/amt-4-1937-2011, 2011.

Kontogeorgis, G. M., Fredenslund, A., and Tassios, D. P.: Simple activity-coefficient model for the prediction of solvent activities in polymer-solutions, Ind. Eng. Chem. Res., 32, 362-372, https://doi.org/10.1021/ie00014a013, 1993.

Krechmer, J. E., Day, D. A., and Jimenez, J. L.: Always lost but never forgotten: Gas-phase wall losses are important in all Teflon environmental chambers, Environ. Sci. Technol., 54, 12890-12897, https://doi.org/10.1021/acs.est.0c03381, 2020.

Krechmer, J. E., Pagonis, D., Ziemann, P. J., and Jimenez, J. L.: Quantification of gas-wall partitioning in Teflon environmental chambers using rapid bursts of low-volatility oxidized species generated in situ, Environ. Sci. Technol., 50, 5757-5765, https://doi.org/10.1021/acs.est.6b00606, 2016.

Kristensen, K., Jensen, L. N., Glasius, M., and Bilde, M.: The effect of sub-zero temperature on the formation and composition of secondary organic aerosol from ozonolysis of alpha-pinene, Environ. Sci.-Proc. Imp., 19, 1220-1234, https://doi.org/10.1039/c7em00231a, 2017.

311 Kroll, J. H., Chan, A. W. H., Ng, N. L., Flagan, R. C., and Seinfeld, J. H.: Reactions of semivolatile organics and their effects
312   on secondary organic aerosol formation, Environ. Sci. Technol., 41, 3545-3550, https://doi.org/10.1021/es062059x, 2007.

313 Li, Y. T., He, L. K., Xie, D., Zhao, A. Q., Wang, L. X., Kreisberg, N. M., Jayne, J., and Liu, Y. J.: Strong temperature influence
314   and indiscernible ventilation effect on dynamics of some semivolatile organic compounds in the indoor air of an office,
315   Environ. Int., 165, 107305, https://doi.org/10.1016/j.envint.2022.107305, 2022a.

316 Li, Y. T., Xie, D., He, L. K., Zhao, A. Q., Wang, L. X., Kreisberg, N. M., Jayne, J., and Liu, Y. J.: Dynamics of di-2-ethylhexyl
317   phthalate (DEHP) in the indoor air of an office, Build. Environ., 223, 109446,
318   https://doi.org/10.1016/j.buildenv.2022.109446, 2022b.

319 Matsunaga, A. and Ziemann, P. J.: Gas-wall partitioning of organic compounds in a Teflon film chamber and potential effects
320   on reaction product and aerosol yield measurements, Aerosol Sci. Technol., 44, 881-892,
321   https://doi.org/10.1080/02786826.2010.501044, 2010.

322 Mattila, J. M., Li, E. Y., and Offenberg, J. H.: Tubing material considerably affects measurement delays of gas-phase
323   oxygenated per- and polyfluoroalkyl substances, J. Air Waste Manage. Assoc., 73, 335-344,
324   https://doi.org/10.1080/10962247.2023.2174612, 2023.

325 McMurry, P. H. and Grosjean, D.: Gas and aerosol wall losses in Teflon film smog chambers, Environ. Sci. Technol., 19,
326   1176-1182, https://doi.org/10.1021/es00142a006, 1985.

327 Nakao, S., Shrivastava, M., Anh, N., Jung, H., and Cocker, D., III: Interpretation of secondary organic aerosol formation from
328   diesel exhaust photooxidation in an environmental chamber, Aerosol Sci. Technol., 45, 964-972,
329   https://doi.org/10.1080/02786826.2011.573510, 2011.

330 Ng, N. L., Chhabra, P. S., Chan, A. W. H., Surratt, J. D., Kroll, J. H., Kwan, A. J., McCabe, D. C., Wennberg, P. O., Sorooshian,
331   A., Murphy, S. M., Dalleska, N. F., Flagan, R. C., and Seinfeld, J. H.: Effect of NO$_x$ level on secondary organic aerosol
332   (SOA) formation from the photooxidation of terpenes, Atmos. Chem. Phys., 7, 5159-5174, https://doi.org/10.5194/acp-
333   7-5159-2007, 2007.

334 Pratap, V., Bian, Q. J., Kiran, S. A., Hopke, P. K., Pierce, J. R., and Nakao, S.: Investigation of levoglucosan decay in wood
335   smoke smog-chamber experiments: The importance of aerosol loading, temperature, and vapor wall losses in interpreting
336   results, Atmos. Environ., 199, 224-232, https://doi.org/10.1016/j.atmosenv.2018.11.020, 2019.

337 Pratap, V., Kiran, S. A., Bian, Q., Pierce, J. R., Hopke, P. K., and Nakao, S.: Observation of vapor wall deposition in a smog
338   chamber using size evolution of pure organic particles, Aerosol Air Qual. Res., 20, 2705-2714,
339   https://doi.org/10.4209/aaqr.2020.05.0268, 2020.

340 Quelever, L. L. J., Kristensen, K., Jensen, L. N., Rosati, B., Teiwes, R., Daellenbach, K. R., Perakyla, O., Roldin, P., Bossi,
341   R., Pedersen, H. B., Glasius, M., Bilde, M., and Ehn, M.: Effect of temperature on the formation of highly oxygenated
342   organic molecules (HOMs) from alpha-pinene ozonolysis, Atmos. Chem. Phys., 19, 7609-7625,
343   https://doi.org/10.5194/acp-19-7609-2019, 2019.

Simon, M., Dada, L., Heinritzi, M., Scholz, W., Stolzenburg, D., Fischer, L., Wagner, A. C., Kurten, A., Rorup, B., He, X. C., Almeida, J., Baalbaki, R., Baccarini, A., Bauer, P. S., Beck, L., Bergen, A., Bianchi, F., Brakling, S., Brilke, S., Caudillo, L., Chen, D. X., Chu, B. W., Dias, A., Draper, D. C., Duplissy, J., El-Haddad, I., Finkenzeller, H., Frege, C., Gonzalez-Carracedo, L., Gordon, H., Granzin, M., Hakala, J., Hofbauer, V., Hoyle, C. R., Kim, C., Kong, W. M., Lamkaddam, H., Lee, C. P., Lehtipalo, K., Leiminger, M., Mai, H. J., Manninen, H. E., Marie, G., Marten, R., Mentler, B., Molteni, U., Nichman, L., Nie, W., Ojdanic, A., Onnela, A., Partoll, E., Petaja, T., Pfeifer, J., Philippov, M., Quelever, L. L. J., Ranjithkumar, A., Rissanen, M. P., Schallhart, S., Schobesberger, S., Schuchmann, S., Shen, J. L., Sipila, M., Steiner, G., Stozhkov, Y., Tauber, C., Tham, Y. J., Tome, A. R., Vazquez-Pufleau, M., Vogel, A. L., Wagner, R., Wang, M. Y., Wang, D. S., Wang, Y. H., Weber, S. K., Wu, Y. S., Xiao, M., Yan, C., Ye, P. L., Ye, Q., Zauner-Wieczorek, M., Zhou, X. Q., Baltensperger, U., Dommen, J., Flagan, R. C., Hansel, A., Kulmala, M., Volkamer, R., Winkler, P. M., Worsnop, D. R., Donahue, N. M., Kirkby, J., and Curtius, J.: Molecular understanding of new-particle formation from alpha-pinene between -50 and +25 °C, Atmos. Chem. Phys., 20, 9183-9207, https://doi.org/10.5194/acp-20-9183-2020, 2020.

Song, C., Na, K. S., and Cocker, D. R.: Impact of the hydrocarbon to NO_x ratio on secondary organic aerosol formation, Environ. Sci. Technol., 39, 3143-3149, https://doi.org/10.1021/es0493244, 2005.

Voigtlaeander, J., Duplissy, J., Rondo, L., Kuerten, A., and Stratmann, F.: Numerical simulations of mixing conditions and aerosol dynamics in the CERN CLOUD chamber, Atmos. Chem. Phys., 12, 2205-2214, https://doi.org/10.5194/acp-12-2205-2012, 2012.

Wang, M. Y., Xiao, M., Bertozzi, B., Marie, G., Rorup, B., Schulze, B., Bardakov, R., He, X. C., Shen, J. L., Scholz, W., Marten, R., Dada, L., Baalbaki, R., Lopez, B., Lamkaddam, H., Manninen, H. E., Amorim, A., Ataei, F., Bogert, P., Brasseur, Z., Caudillo, L., De Menezes, L. P., Duplissy, J., Ekman, A. M. L., Finkenzeller, H., Carracedo, L. G., Granzin, M., Guida, R., Heinritzi, M., Hofbauer, V., Hohler, K., Korhonen, K., Krechmer, J. E., Kurten, A., Lehtipalo, K., Mahfouz, N. G. A., Makhmutov, V., Massabo, D., Mathot, S., Mauldin, R. L., Mentler, B., Muller, T., Onnela, A., Petaja, T., Philippov, M., Piedehierro, A. A., Pozzer, A., Ranjithkumar, A., Schervish, M., Schobesberger, S., Simon, M., Stozhkov, Y., Tome, A., Umo, N. S., Vogel, F., Wagner, R., Wang, D. S., Weber, S. K., Welti, A., Wu, Y. S., Zauner-Wieczorek, M., Sipila, M., Winkler, P. M., Hansel, A., Baltensperger, U., Kulmala, M., Flagan, R. C., Curtius, J., Riipinen, I., Gordon, H., Lelieveld, J., El-Haddad, I., Volkamer, R., Worsnop, D. R., Christoudias, T., Kirkby, J., Mohler, O., and Donahue, N. M.: Synergistic HNO_3-H_2SO_4-NH_3 upper tropospheric particle formation, Nature, 605, 483-489, https://doi.org/10.1038/s41586-022-04605-4, 2022.

Yeh, G. K. and Ziemann, P. J.: Alkyl nitrate formation from the reactions of C_8-C_{14} n-alkanes with OH radicals in the presence of NO_x: Measured yields with essential corrections for gas-wall partitioning, J. Phys. Chem. A, 118, 8147-8157, https://doi.org/10.1021/jp500631v, 2014.

Yeh, G. K. and Ziemann, P. J.: Gas-wall partitioning of oxygenated organic compounds: Measurements, structure-activity relationships, and correlation with gas chromatographic retention factor, Aerosol Sci. Technol., 49, 726-737, https://doi.org/10.1080/02786826.2015.1068427, 2015.

378   Yu, S., Jia, L., Xu, Y., Zhang, H., Zhang, Q., and Pan, Y.: Wall losses of oxygenated volatile organic compounds from
379   oxidation of toluene: Effects of chamber volume and relative humidity, J. Environ. Sci., 114, 475-484,
380   https://doi.org/10.1016/j.jes.2021.09.026, 2022.

381   Zhang, X., Cappa, C. D., Jathar, S. H., McVay, R. C., Ensberg, J. J., Kleeman, M. J., and Seinfeld, J. H.: Influence of vapor
382   wall loss in laboratory chambers on yields of secondary organic aerosol, Proc. Natl. Acad. Sci. U. S. A., 111, 5802-5807,
383   https://doi.org/10.1073/pnas.1404727111, 2014.

384   Zhang, X., Schwantes, R. H., McVay, R. C., Lignell, H., Coggon, M. M., Flagan, R. C., and Seinfeld, J. H.: Vapor wall
385   deposition in Teflon chambers, Atmos. Chem. Phys., 15, 4197-4214, https://doi.org/10.5194/acp-15-4197-2015, 2015.

386   Zhao, Y. L., Kreisberg, N. M., Worton, D. R., Teng, A. P., Hering, S. V., and Goldstein, A. H.: Development of an in situ
387   thermal desorption gas chromatography instrument for quantifying atmospheric semi-volatile organic compounds,
388   Aerosol Sci. Technol., 47, 258-266, https://doi.org/10.1080/02786826.2012.747673, 2013.

Nomenclature

A table that contains the definitions of parameters and corresponding units.

k_1 forward rate constant (s^{-1})

k_{-1} backward rate constant (s^{-1})

k_2 first-order loss rate constant (s^{-1})

$\tau_{surface}$ gas-surface equilibrium time scale (min)

τ_{inner} diffusion time scale (min)

C_0 initial SVOC concentration in gas phase (µg m^{-3})

C_{gas} SVOC concentration in gas phase (µg m^{-3})

C_{wall} SVOC concentration on wall surface (µg m^{-3})

K_{eq} gas-surface equilibrium constant

$C_{FEP\_surface}$ equivalent organic mass concentration of the FEP chamber surface (mg m^{-3})

M_{wall} average molecular mass of the Teflon wall (g mol^{-1})

$\gamma_{FEP\_surface}$ activity coefficient in the Teflon surface

R gas constant (J K^{-1} mol^{-1})

T temperature (K)

$P_s(T)$ saturation vapor pressure of compound at temperature T (Pa)
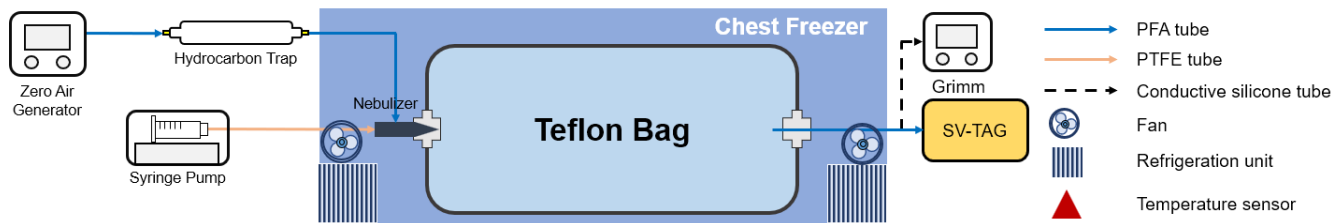
406

407   **Figure 1.** Schematic diagram of the experimental setup.

408
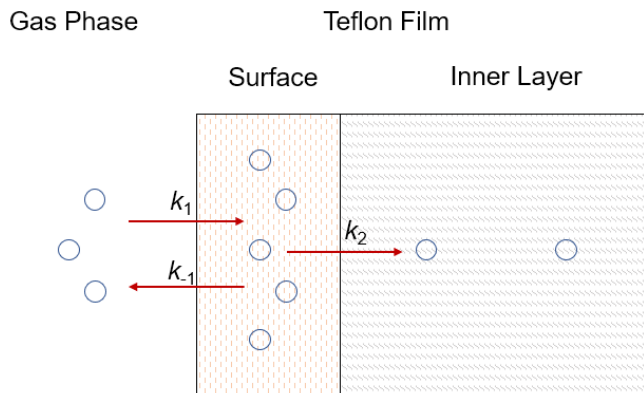
Figure 2. Schematic diagram of wall loss process. Compounds partition between gas phase and surface layer with forward
and backward rates (k_1 and k_{-1}). Compounds in surface layer undergo irreversible diffusion into inner layer with first-order
loss rate (k_2).

412
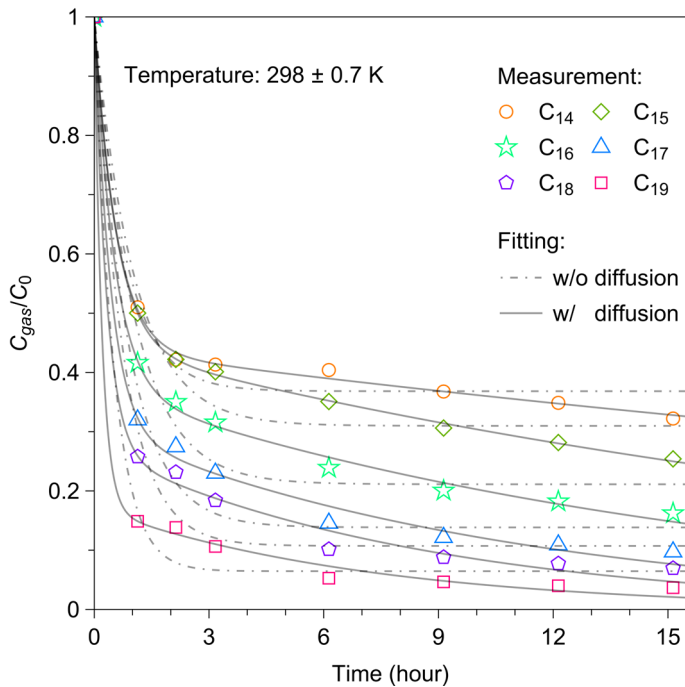
Figure 3. Temporal variation in C_{gas}/C_0 for C_{14}-C_{19} n-alkanes at 298 ± 0.7 K following injection. C_{gas} is the concentration of each n-alkane in the gas phase, and C_0 is the corresponding initial concentration of each n-alkane. The two-layer kinetic sorption model (Section 2.2) was employed to fit the data (black solid line). The black dot-dashed lines show the fitting result to the model that ignores the diffusion process to the inner layer (*i.e.*, $k_2 = 0$).
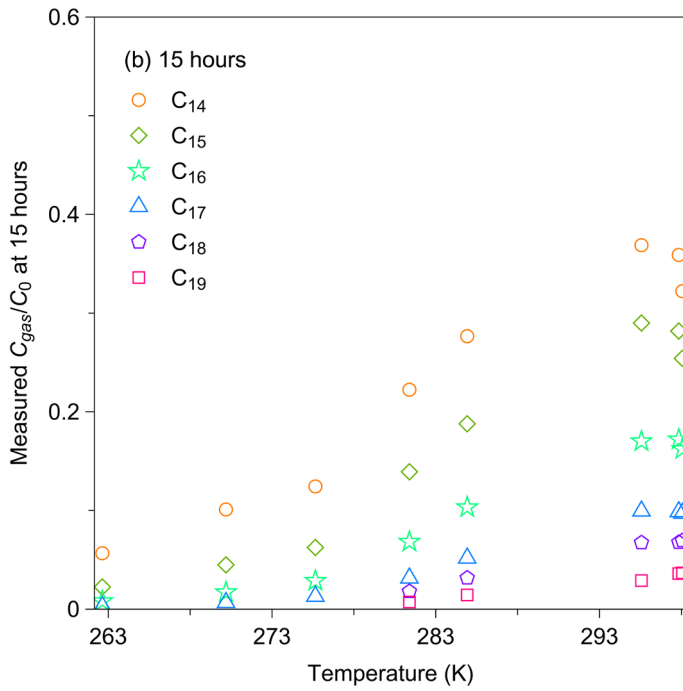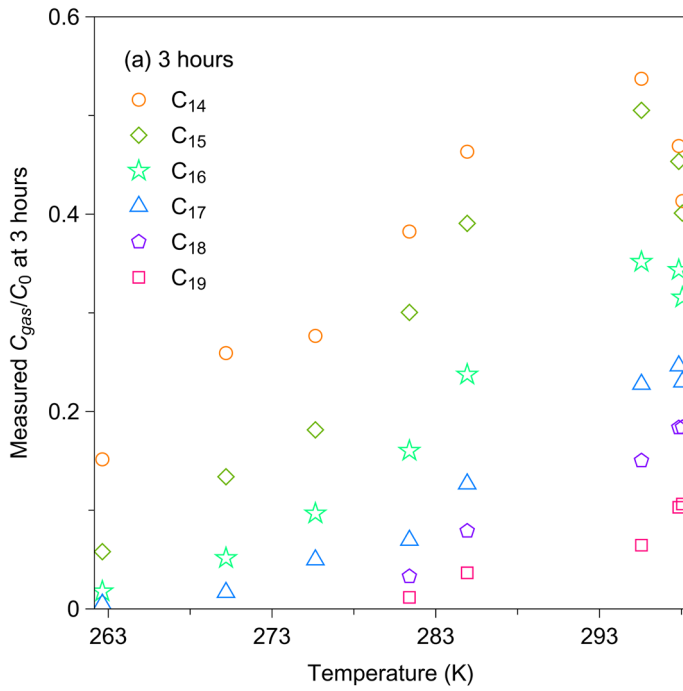
417

418 **Figure 4.** Measured values of C_{gas}/C_0 at (a) 3 hours and (b) 15 hours after injection.

419
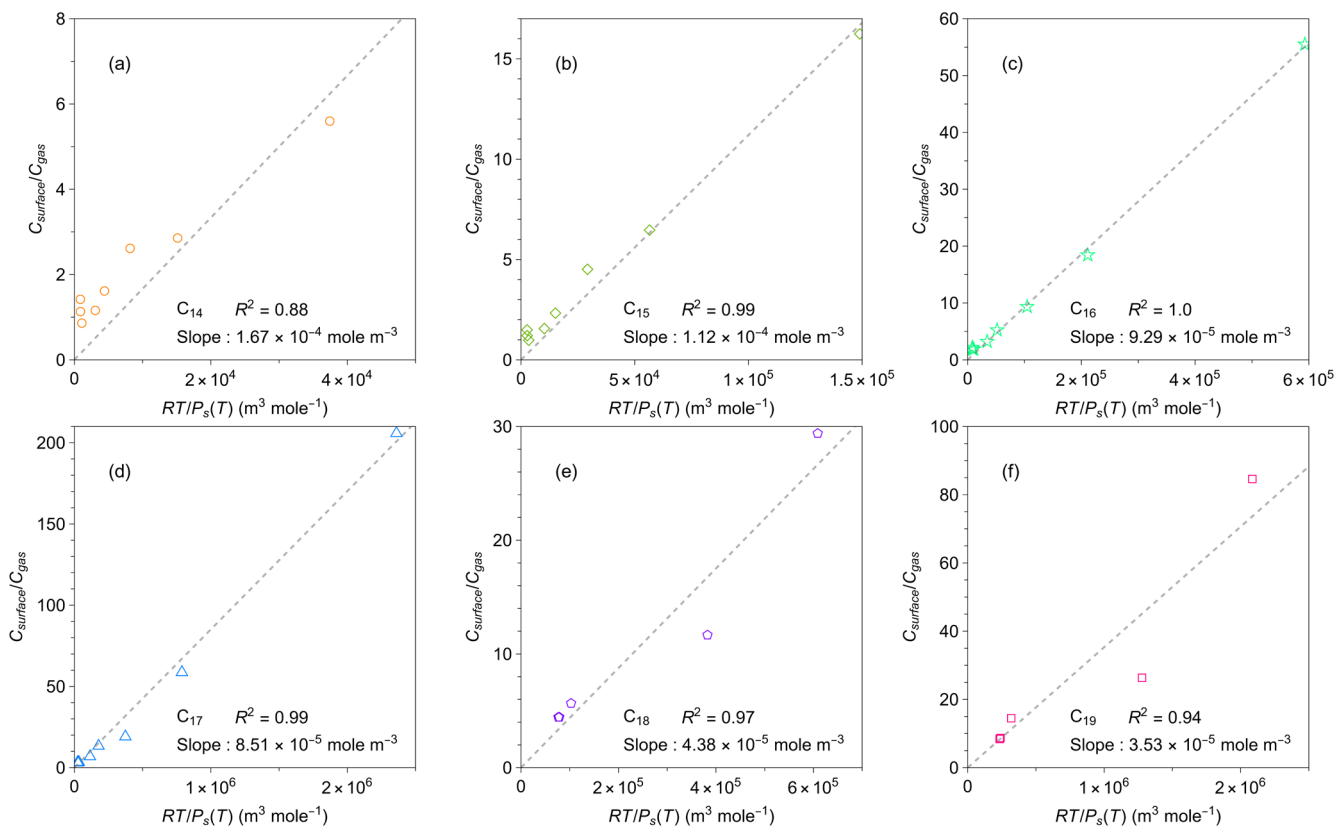
Figure 5. Relationships between measured ratio of concentrations in the chamber wall surface phase and in the gas phase at quasi-equilibrium and calculated values of $RT/P_s(T)$ for individual n-alkanes. Calculation methods for $C_{surface}/C_{gas}$ is detailed in the text. The values of $RT/P_s(T)$ for each n-alkane were calculated by the EVAPORATION group contribution method (Compernolle et al., 2011). The black dashed lines are best linear fits of the data for each n-alkane.

424
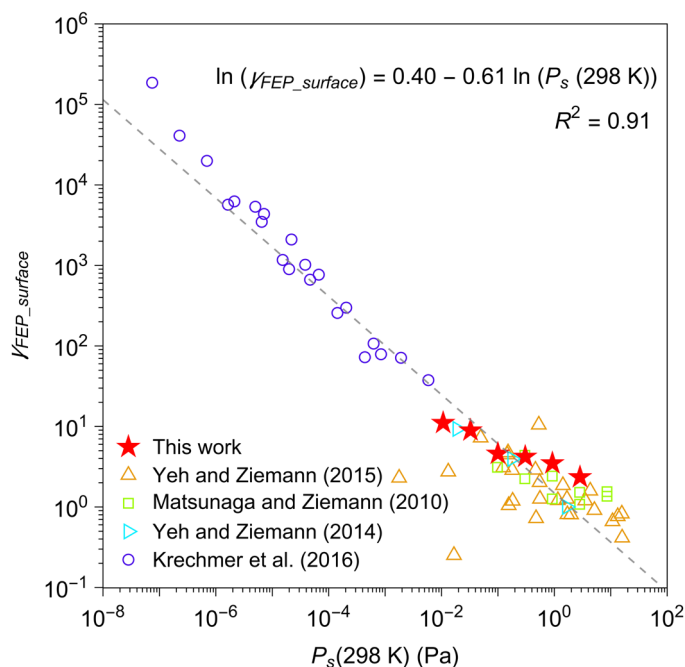
Figure 6. Activity coefficient ($\gamma_{FEP\_surface}$) of organic compounds in FEP film. The sources of data include this work and the literature (compiled by Huang et al. (2018b), including Matsunaga and Ziemann (2010), Yeh and Ziemann (2014, 2015), and Krechmer et al. (2016)). A list of chemical species that were investigated by each study is available in Table S4. Saturation vapor pressures at 298 K (P_s(298 K)) were estimated by EVAPORATION (Compernolle et al., 2011).

429
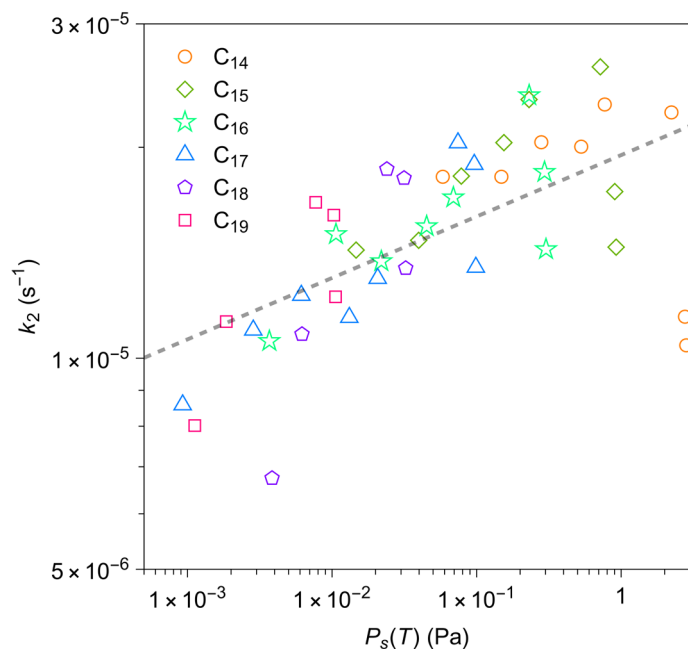
Figure 7. Relationship between calculated first-order loss rate k_2 for each *n*-alkane and calculated values of saturation vapor
pressure by the EVAPORATION group contribution method (Compernolle et al., 2011). The calculation method for k_2 is
detailed in the text. The black dashed line is the best linear fit to the data in a logarithmic scale.